

## Architecture of functional lateralisation in the human brain

**Karolis V<sup>a,b\*</sup>, Corbetta M<sup>c-g</sup> & Thiebaut de Schotten M<sup>a,b,h\*</sup>**

<sup>a</sup> Brain Connectivity and Behaviour Group, Sorbonne Universities, Paris France.

<sup>b</sup> Frontlab, Institut du Cerveau et de la Moelle épinière (ICM), UPMC UMRS 1127, Inserm U 1127, CNRS UMR 7225, Paris, France.

<sup>c</sup> Department of Neurology, Washington University Saint Louis, USA □

<sup>d</sup> Department of Radiology, Washington University Saint Louis, USA □ <sup>e</sup> Department of Neuroscience, Washington University Saint Louis, USA □

<sup>e</sup> Department of Biomedical Engineering, Washington University Saint Louis, USA

<sup>f</sup> Department of Neuroscience, University of Padova, Italy □

<sup>g</sup> Padova Neuroscience Center, University of Padova, Italy

<sup>h</sup> Groupe d'Imagerie Neurofonctionnelle, Institut des Maladies Neurodégénératives-UMR 5293, CNRS, CEA University of Bordeaux, Bordeaux, France

\* Corresponding authors [slava.karolis@kcl.ac.uk](mailto:slava.karolis@kcl.ac.uk) and [michel.thiebaut@gmail.com](mailto:michel.thiebaut@gmail.com)

## **Abstract**

Functional lateralisation is a fundamental principle of the human brain. However, a comprehensive taxonomy of functional lateralisation and its organization in the brain is missing. We report the first complete map of functional hemispheric asymmetries in the human brain, reveal its low dimensional structure, and its relationship with structural inter-hemispheric connectivity. Our results suggest that the lateralisation of brain functions is distributed along four functional axes: symbolic communication, perception/action, emotion, and decision-making, and that cortical regions which show that asymmetries in task-evoked activity have reduced connections with the opposite hemisphere.

“Are you left- or right-brain?”. The widespread belief that hemispheric dominance influences the human character and habits comes from the misinterpretation of decades-long neuropsychological findings<sup>1</sup>. This research demonstrated functional lateralisation as a fundamental principle of brain’s organisation<sup>2-4</sup>. Today, informed by neuroimaging measures, theories on functional lateralisation suggest a less radical organisation and assume that the two hemispheres balance each other<sup>5</sup>. Despite the implications of functional lateralisation theories for neurodevelopmental and psychiatric disorders<sup>6,7</sup>, as well as for stroke recovery<sup>8,9</sup>, a comprehensive mapping of lateralised cognitive functions is, to our knowledge, still missing in the literature. Furthermore, the mechanisms sustaining functional lateralisation, such as the communication between the hemispheres remains an open debate<sup>10,11</sup>.

The contribution of the corpus callosum, the most considerable interhemispheric connection, to the emergence of functional lateralisation arise from two different ideas<sup>12</sup>. The first hypothesis suggests that, during evolution, brain size expansion led to functional lateralisation to avoid excessive conduction delays between the hemispheres<sup>13</sup>. Accordingly, functionally lateralised regions will be connected less strongly via corpus callosum connections than non-lateralised regions to function efficiently<sup>14</sup>. The second hypothesis proposes that functional lateralisation arises from the competition between the hemispheres that inhibits each other via the corpus callosum. As functionally lateralised regions would need to inhibit more the opposite hemisphere than non-lateralised regions, they could be more connected by the corpus callosum. Preliminary anatomical<sup>15</sup> and fMRI<sup>16</sup> studies provide support for both theories. However, the small range of functions investigated and shortcomings in the methods often limit the interpretability of the findings<sup>11</sup>. Overall, the generalisation of these theories and findings to the whole brain functional organisation remains unknown.

Here, we took advantage of the largest fMRI meta-analytic dataset<sup>17</sup> with the highest quality structural connectivity data<sup>18</sup> to produce, for the first time, a comprehensive mapping of functional lateralisation, demonstrate its low dimensional structure, and examine its relationship with corpus callosum connectivity.

## Results

### Global structure of functional lateralisation

We selected terms related to specific cognitive processes out of the whole Neurosynth database (see **Supplementary Table 1**).

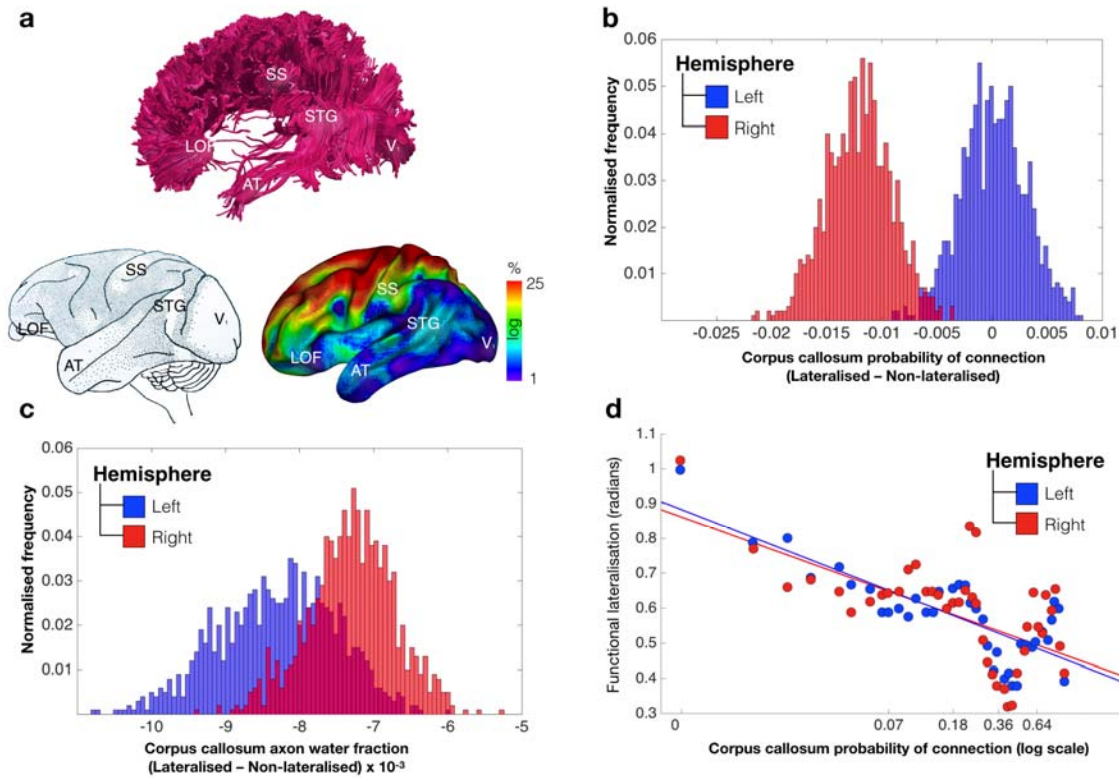
After correction for anatomical differences between the left and the right hemispheres<sup>19</sup>, a functional lateralisation map was computed for each term to compare voxels between hemispheres. A varimax-rotated principal component analysis indicated that 171 principal components (PCs with eigenvalues higher than the grand average) explained 72.6 % of the variance of the lateralisation maps. General linear modelling was subsequently employed with PCs loads as a set of predictors to fit LI maps data and identify voxels with a significant lateralisation associated with each component. After 5000 permutations 25 PCs showed voxels with a significant lateralisation (>20 voxels;  $P < 0.05$  family-wise error corrected) (see **Supplementary Table 2**).

Next, a multivariate spectral embedding ordered the lateralisation maps spatially according to their similarity. As a first step, **Figure 1a** (see also **Supplementary Figure 1**) shows the embedding in the first two dimensions. It reveals a triangular organisation of the lateralisation maps with three vertices: symbolic communication, perception/action, and emotion. A t-ratio test<sup>20</sup> confirmed the statistical veracity of such triangular organisation. Next, we used the same analysis to explore other dimensions and revealed a 4<sup>th</sup> vertex given by decision making (**Figure 1b** and **Supplementary Figure 2**).



random subsets of non-lateralised voxels, for each hemisphere separately. The number of voxels in each subset was equal to the number of lateralised voxels. We then constructed the connectivity distribution of non-lateralised regions by calculating an average corpus callosum probability of connection for each sample. These values were subtracted from the average connectivity value of lateralised voxels in the corresponding hemispheres. Figure 2a demonstrates that lateralised regions in the right hemisphere have a lower probability of connection with the corpus callosum than non-lateralised regions. However, there was no difference between lateralised and non-lateralised regions in the left hemisphere. These results were contingent on the fact that non-lateralised regions have a higher probability of connection with the corpus callosum in the right than the left hemisphere (**Supplementary Figure 3**).

As probability of connections estimates derived from diffusion weighted imaging have well known methodological shortcomings<sup>24</sup>, we replicated the same analysis by sampling axonal water fraction in the mid-section of the corpus callosum respectively for lateralised maps and subsets of non-lateralised voxels. **Figure 2c** indicates axonal water fraction was consistently lower for corpus callosum voxels projecting onto lateralised regions when compared to non-lateralised voxels. Additionally, the plots suggested a slightly lower axonal water fraction for left hemisphere regions as compared to the right hemisphere.



**Figure 2.** Lateralisation and inter-hemispheric connectivity (a) Tractography of the corpus callosum in a representative subject (top), cortical projection of the corpus callosum derived from axonal tracing in monkeys<sup>25</sup> (bottom left), cortical projections of the corpus callosum derived from tractography in humans (bottom right). (b) Binary chart of the difference between lateralised and non-lateralised regions in the corpus callosum probability of connection. (c) Binary chart of the difference between lateralised and non-lateralised regions in the corpus callosum axonal water fraction. (d) Dimensional relationship between the degree of functional lateralisation and the corpus callosum probability of connectivity.

The degree of functional lateralisation (see Methods section for the definition of the measure), can vary—from a unilateral to a relatively asymmetric pattern of activity. In the latter case, both hemispheres are involved in a function, but one is more active than the other. Therefore, we explored whether a proportional relationship existed between the degree of functional lateralisation and the probability of corpus callosum connectivity. **Figure 2d** indicates a negative relationship between the probability of and the degree of functional lateralisation, both for the left and the right hemisphere ( $r = -.81$  and  $r = -.69$ , respectively,  $p < .001$ ). Furthermore, we repeated the same analysis regressing out the average level of activity in

functionally lateralised areas. The relationship between the level of functional dominance and the probability of connection to corpus callosum remained unchanged for the left hemisphere ( $r = -.79$ ) and increased for the right hemisphere ( $r = -.87$ ).

## Discussion

In the present study, we provide for the first time a comprehensive mapping of the brain functional lateralisation. Results indicated a low-dimensional structure of functional lateralisation along four axes. Additionally, lateralised regions were characterised by reduced corpus callosum connectivity compared to areas without a distinct functional lateralisation. Finally, within the pool of lateralised regions, inter-hemispheric connectivity was proportionally associated to the degree of the hemispheric functional dominance.

Based on the meta-analysis of the task-related functional magnetic resonance literature we have been able to replicate several classical functional lateralisation profiles. Most notably, language was dominant in prefrontal and superior temporal regions of the left hemisphere<sup>26</sup>. Attention, a cognitive function typically showing right hemisphere functional specialization<sup>19,27</sup>, was not associated with a lateralised component in our study. However, it had a strong negative weighting on the language component, indicating as previously reported a balance between language and attention in similar brain regions<sup>28</sup>. Some of the lateralisation maps presented an opponent lateralisation in the cerebellum, which supports well the theory of the opposite laterality of cerebellar function for high cognitive functions<sup>29,30</sup>. Pairs of oppositely lateralised regions in cerebrum and cerebellum were in a remarkable agreement with findings derived from tracing studies<sup>31</sup>. For instance, area Crus II, which showed a significant right lateralisation for the language component in the cerebellum is connected to frontal regions involved in language; similarly, Areas V/VI and VIIIb, showing significant right lateralisation movement and finger components, are connected to the left sensorimotor cortical regions. These findings support the validity and the anatomical precision of the functional lateralisation maps based on fMRI meta-analyses.

The overall functional lateralisation of the brain demonstrated a low-dimensional structure along four axes corresponding to their respective contribution to symbolic communication, perception/action, emotion, and decision making. The triangular organisation represents a certain interest as it may be related to the concept of Pareto optimality. In evolutionary biology<sup>20</sup>, the concept presumes that distribution of traits across species demonstrates a



trade-off: a prominence of a particular trait in a species exists at a cost of other traits being relatively silent. This gives a rise to a triangular organisation of traits across species, known as a Pareto front, with the apices of the triangles which encompass the trait distribution (“Pareto front”) known as archetypes. Our result therefore indicates that a trade-off between lateralisation brain states exists and there are four archetypical states of brain lateralisation. This result supports previous findings reporting a low dimensionality of functional networks<sup>32</sup> and of behavioural manifestations existing in both healthy controls<sup>33,34</sup> and patients<sup>35</sup>, whereby individual performances or deficits are not task-specific but instead shared across a range of cognitive tasks. For example, in stroke patients, two axes of behavioural deficits, one related to language and the other to attention-motor functions exist<sup>36</sup>. Our result suggests that, at least in stroke, two supplementary axis of deficit might exist along the emotional<sup>37,38</sup> and decision making<sup>39</sup> dimensions and are under-represented by the standard behavioural and cognitive examinations. Additionally, the similarity between the grand scale organisation of functional lateralisation in healthy controls and behavioural deficits suggest the importance of inter-hemispheric connections in recovery from stroke as shown recently by several studies<sup>40,41</sup>.

The distribution of the probability of connection of the corpus callosum onto the brain surface matched the previous atlases derived from interhemispheric homotopic functional connectivity analyses<sup>42</sup>. Time and energy costs are required to integrate information across hemispheres. Therefore, the role of inter-hemispheric connectivity for functional lateralisation has long been debated in the literature<sup>43</sup>. The current study presents a comprehensive demonstration that functional lateralisation is linked to a decrease of callosal function<sup>12</sup>, possibly through the mechanisms of callosal myelination and pruning<sup>44</sup>. Hypothetically, this reduced inter-hemispheric communication would optimise the treatment time in the brain at the expense of a decreased capacity of recovery after a brain injury.

However, it is important to stress that several factors limited the interpretation of the findings. For instance, while the meta-analytic approach has the power to summarise thousands of task-related fMRI findings, it is limited by publication biases which prevent to generalise the current findings to all brain functions<sup>45</sup>. The limitations of the connectivity analyses derived from diffusion-weighted imaging<sup>46</sup> also prevented us from investigating with confidence the distinct contribution of homotopic and heterotopic areas to the functional lateralisation. The advent of new diffusion imaging methods<sup>47</sup>, as well as post-mortem investigation<sup>48</sup>, might circumvent this bias in the future.

In conclusion, the present analysis provides us with a comprehensive view of functional lateralisation in humans, which mostly concerns symbolic communication, perception/action, emotion-related and decision-making functions. It also reveals some of its mechanisms such as the relationship between functional lateralisation and the strength of communication between the hemispheres. The similarity between the current findings and recent work on neurological symptoms bring up new hypotheses on the mechanisms supporting brain recovery after a brain lesion.

## Methods

### Datasets

In this study we used a meta-analytic approach to functional MRI studies described by Yarkoni et al. (2011; <http://neurosynth.org>). We downloaded the Neurosynth database containing, as of the 25th of September 2017, 3107 reverse unthresholded functional maps, as well as the details of 11406 literature sources for the maps and 3107 x 11406 terms loadings.

Structural connectivity data were obtained from the Human Connectome Project 7T dataset of young adults (<http://www.humanconnectome.org/study/hcp-young-adult/>) (WU-Minn Consortium; Principal Investigators: David Van Essen and Kamil Ugurbil; 1U54MH091657) funded by the 16 NIH Institutes and Centers that support the NIH Blueprint for Neuroscience Research; and by the McDonnell Center for Systems Neuroscience at Washington University. The scanning parameters have previously been described in Vu et al. <sup>49</sup>.

### Data pre-processing

#### A) Neurosynth data

Two researchers (V.K & M.TdS) acted as judges selecting terms which in their view related to specific cognitive processes. The selection procedure was two-stage. At the first stage, the judges made their selection independently. Brain anatomical (e.g., “salience network”), psychiatric (e.g., “schizophrenia”), or pathological (e.g., “alzheimer”) terms were systematically excluded. The two judges agreed on 422 terms as related to cognitive processes and on 2309 terms as unrelated, hence to be discarded (88% reproducibility). For the other terms, the judges made their decision together. In the end, 590 cognitive terms were selected for the study.

Given that the Neurosynth functional maps are provided in the standard 2mm MNI template space, which is not symmetric, we co-registered non-linearly the MNI template to a MNI symmetrical template, available at <http://www.bic.mni.mcgill.ca/ServicesAtlases/ICBM152NLin2009>, using the Greedy symmetric diffeomorphic normalization (GreedySyN) pipeline distributed with the Advanced Normalization Tools (<http://stnava.github.io/ANTs/>) <sup>50</sup>. The symmetrical template was downsampled to a 2 mm voxel size to match the voxel dimensions of the standard template.

The estimated transformation between non-symmetrical and symmetrical MNI spaces were then applied to all functional maps.

The following steps were performed to obtain lateralisation indices for each functional map following their co-registration with symmetrical template. Firstly, we split the functional maps into the left- and right-hemisphere parts and smoothed the resulting maps using a 6 mm FWHM Gaussian filter. We then flipped the left-hemisphere maps and subtracted them from unflipped right-hemisphere maps in order to obtain laterality indices (LI) maps (see <sup>19</sup> for a similar approach). Positive and negative values in these maps would signify a higher meta-analytic evidence for, respectively, right and left lateralisation of the function associated with a term.

## **B) Structural connectome data**

The following pre-processing steps have been applied to the HCP dataset. Firstly, the images were corrected for signal drift motion and eddy current artefacts using ExploreDTI toolbox for Matlab (<http://www.exploredti.com> <sup>51, 52</sup>). ExploreDTI has also been used to extract estimates of axonal water fraction <sup>23</sup>. Whole-brain deterministic tractography was performed in the native DWI space using StarTrack software (<http://www.natbrainlab.com>). A damped Richardson-Lucy algorithm was applied for spherical deconvolutions <sup>53</sup>. A fixed fibre response corresponding to a shape factor of  $\alpha = 1.5 \times 10^{-3} \text{ mm}^2/\text{s}$  was adopted, coupled with the geometric damping parameter of 8. Two hundred algorithm iterations were run. The absolute threshold was defined as 3 times the spherical fibre orientation distribution (FOD) of a grey matter isotropic voxel and the relative threshold as 8% of the maximum amplitude of the FOD <sup>54</sup>. A modified Euler algorithm <sup>55</sup> was used to perform the whole brain streamline tractography, with an angle threshold of  $35^\circ$ , a step size of 0.625mm, and a minimum streamline length of 15mm.

In order to co-register the structural connectome data to the standard MNI 2mm space, the data were converted into streamline density volumes where the intensities were given by the number of streamlines traversing each voxel. The study-specific template of streamline density volumes was generated using the Greedy symmetric diffeomorphic normalisation (GreedySyN) pipeline distributed with the Advanced Normalisation Tools (<http://stnava.github.io/ANTs> <sup>50</sup>). After an initial linear realignment of images, four iterations

of the nonlinear template creation were performed. The template was then co-registered with a standard 2mm MNI152 template using flirt tool implemented in FSL. The affine and diffeomorphic transformations between native DWI spaces and the standard MNI space were subsequently applied to the individual connectomes and axonal water fraction maps. The trackmath tool distributed with the software package Tract Querier<sup>56</sup> was used for the registration of connectome data. In the end, the data of 163 participants were available for the analyses.

## **Statistical analyses of laterality (see Supplementary Figure 4)**

### **A) Determination of lateralisation maps**

The construction of brain's functional lateralisation maps was completed in two steps. In the first step, we sought to address the redundancy while preserving the richness of the Neurosynth data. For instance, many selected terms were related as singular and plural forms of the same word (e.g, “visual form” and “visual forms”) and therefore their maps are likely to be very similar. To address this issue we grouped the terms on the basis of their similarities using a varimax-rotated principal component (PC) analysis implemented in SPSS (SPSS, Chicago, IL). Following a standard principal component analysis, 171 extracted orthogonal components with eigenvalues more than the grand average were submitted to the varimax-rotation procedure using Kaiser normalisation criterion<sup>57</sup>, with a maximum of 1000 iterations for convergence.

In the second step, a general linear modelling was employed to identify voxels with a significant lateralisation associated with a particular component. In this analysis, the PC were used as a set of predictors to fit LI maps data and obtain beta maps. The permutation test was performed to identify significantly lateralised regions. Given that varimax rotation may impose correlations between the columns of the PC matrix, we performed permutation on the rows of the unrotated matrix, subsequently applying component rotation and calculating the beta maps for each permutation. This procedure allowed us to mimic the correlational structure of the unpermuted data and provide a more robust test of significance. In order to account for multiple comparisons, the maximal statistics approach was used whereby the beta values for the real data were compared to the maximal (either positively or negatively) beta values estimated on each permutation across all voxels. 5000 permutations were run. The

voxels were considered as showing a significant lateralisation if they simultaneously satisfied two criteria: 1) their beta values were in 97.5% cases higher or lower than, respectively, maximal positive and negative beta values obtained via permutations (i.e.,  $p < .05$ , two-tailed and FWE-corrected); 2) they formed a cluster of at least 20 voxels. The second criterion was used to exclude small and possibly spurious effects observed in a small number of voxels.

## **B) Determination of non-lateralised regions**

To enable a comparison between lateralised regions and regions without a significant lateralisation, the latter were identified by repeating the analyses outlined in the previous section for the left and right hemispheres separately. The clusters which passed the significance threshold at least for one component and one hemisphere, and non-overlapping with lateralised regions, were taken to denominate the regions without significant lateralisation (“non-lateralised regions”).

## **C) Multivariate embedding**

In order to characterise the low dimensionality of functional brain lateralisation, a spectral embedding of the LI maps was performed using eigen decomposition of graph normalised Laplacian of similarity matrix<sup>58</sup>. This similarity matrix was obtained as follows. Firstly, the functional maps values were de-noised, in a sense that it contained the values accounted for by the linear combination of 171 PCs. Secondly, the elements of the similarity matrix were calculated as dot products across all voxels for all pairs of maps. Negative values were zeroed to permit estimability. The embedding dimensions were ordered according to their eigen values, from small to large. The first, non-informative, dimension associated with a zero eigen value was dropped. An emerging triangular structure was quantified as a t-ratio, i.e., a ratio between the area of the convex hull encompassing all points in embedded space and an encompassing triangle of a minimal area<sup>20</sup>. These values were compared to the t-ratios of random LI maps. The latter were obtained by generating via permutation 2000 sets of 590 left-right random pairs. For each set, random LI maps were calculated for each pair and then submitted to varimax analysis with the number of PCs = 171. The embedding procedure was identical to the procedure applied to non-random LI maps. The dimensional span of triangular organisation was evaluated by testing if t-ratio for non-random LI maps was greater than t-

ratios of random LI maps in each 2-dimensional subspace of embedding ( $p < .05$ , Bonferroni-corrected).

## **Analyses of function-structure relationship (see Supplementary Figure 5)**

### **A) Measures of the connectivity strength**

We combined lateralisation maps and structural connectivity by first projecting lateralised maps, irrespective of the left and right polarity of lateralisation, onto white matter boundary of non-symmetrical MNI template, determining the overlapping voxels and subsequently by seeding tractography from these voxels to the corpus callosum.

Two measures for the strength of structural inter-hemispheric connectivity were analysed. Macrostructurally, the strength of connectivity was measured in terms of replicability<sup>22</sup> of a connection between a seeded voxel and corpus callosum across the HCP sample. In other words, this measure represents a ratio of the number of participants in which a connection exists between a seeded voxel and the corpus callosum to the overall HCP sample size. A connection was classified as existing if tractography seeded from a voxel in a participant's brain generated at least one streamline passing through any voxel situated in the corpus callosum. We will refer to this measure as a “probability of connection”.

The second, microstructural, measure referred to the axonal water fraction in the voxels of corpus callosum which were hit by streamlines from the seeded lateralised (or non-lateralised) regions. This measure was calculated as a weighted average of the axonal water fraction of the voxels in the corpus callosum, whereby the weights were calculated as a probability that a voxel in the corpus callosum is connected by at least one streamline to any lateralised voxel in the brain.

The same procedure applied to the calculation of the connectivity measures for non-lateralised regions. The number of non-lateralised voxels was 3.6 times greater than the number of lateralised voxels.

### **B) Comparison of the connectivity between lateralised and non-lateralised regions**

The comparison of connectivity between lateralised and non-lateralised regions was performed by randomly sampling (without replacement) a subset of lateralised voxels and comparing the average connectivity measures of lateralised voxels to the connectivity

measures of the sampled non-lateralised regions. 1000 samples were drawn for each hemisphere separately. The number of voxels in each sample of non-lateralised voxels was equal to the number of lateralised voxels.

### C) **Hemispheric dominance**

The degree of functional hemispheric dominance was evaluated in radians as an arctangent of the ratio between the strengths of activation in two hemispheres.  $\pi/4$  was subtracted from this value to ensure that the absolute magnitude of this value increases if the task activation is unilateral and decreases if both hemispheres demonstrate comparable levels of task activity. Given that a partial spatial overlap between lateralised regions associated with different components is possible, in the analyses we picked the dominance values associated with components which rendered a largest z-score in a particular voxel. In order to obtain robust estimate for the relationship between hemispheric dominance and the strength of inter-hemispheric connectivity, the voxels were binned by the probabilities of connection such that the smallest bin width (given by `logspace` function in Matlab) was of the size equal to  $1/163$  and increased with the probability of connection. This procedure was used to partially compensate for the fact that only a very limited number of voxels had a high probability of connection to corpus callosum, whereas the majority were characterised by small values.



## Authors contribution

V.K. implemented the methods, performed the analyses and wrote the manuscript. M.C. conceived and coordinated the study, and wrote the manuscript. M.T.S. conceived and coordinated the study, reviewed the neuroimaging data, wrote the manuscript, and provided funding.

## Acknowledgments

The research leading to these results received funding from the “Agence Nationale de la Recherche” [grant number ANR-13- JSV4-0001-01]. Additional financial support comes from the program “Investissements d’avenir” ANR-10-IAIHU-06. M.C. was supported by NIH R01NS095741, and a strategic grant from the University of Padua. MC was a visiting professor at the Institut du Cerveau and Moelle Epiniere (ICM) in Paris where the research was conducted.

## References

1. Geschwind, N. & Galaburda, A.M. Cerebral lateralization. Biological mechanisms, associations, and pathology: I. A hypothesis and a program for research. *Arch Neurol* **42**, 428-459 (1985).
2. Sperry, R.W. *Lateral Specialization in the Surgically Separated Hemispheres* (Rockefeller University Press, New York, 1974).
3. Kong, X.Z., *et al.* Mapping cortical brain asymmetry in 17,141 healthy individuals worldwide via the ENIGMA Consortium. *Proc Natl Acad Sci U S A* **115**, E5154-E5163 (2018).
4. Toga, A.W. & Thompson, P.M. Mapping brain asymmetry. *Nat Rev Neurosci* **4**, 37-48 (2003).
5. Herve, P.Y., Zago, L., Petit, L., Mazoyer, B. & Tzourio-Mazoyer, N. Revisiting human hemispheric specialization with neuroimaging. *Trends Cogn Sci* **17**, 69-80 (2013).
6. Wexler, B.E. Cerebral laterality and psychiatry: a review of the literature. *Am J Psychiatry* **137**, 279-291 (1980).
7. Bishop, D.V. Cerebral asymmetry and language development: cause, correlate, or consequence? *Science* **340**, 1230531 (2013).
8. Forkel, S.J., *et al.* Anatomical predictors of aphasia recovery: a tractography study of bilateral perisylvian language networks. *Brain* **137**, 2027-2039 (2014).
9. Lunven, M., *et al.* White matter lesional predictors of chronic visual neglect: a longitudinal study. *Brain* **138**, 746-760 (2015).
10. Hopkins, W.D. & Cantalupo, C. Theoretical Speculations on the Evolutionary Origins of Hemispheric Specialization. *Current Directions in Psychological Science* **17**, 233-237 (2008).
11. Tzourio-Mazoyer, N. *Intra- and Inter-hemispheric Connectivity Supporting Hemispheric Specialization* (Springer, Cham (CH), 2016).
12. Gazzaniga, M.S. Cerebral specialization and interhemispheric communication: does the corpus callosum enable the human condition? *Brain* **123** ( Pt 7), 1293-1326 (2000).

13. Ringo, J.L., Doty, R.W., Demeter, S. & Simard, P.Y. Time is of the essence: a conjecture that hemispheric specialization arises from interhemispheric conduction delay. *Cereb Cortex* **4**, 331-343 (1994).
14. Markov, N.T., *et al.* Cortical high-density counterstream architectures. *Science* **342**, 1238406 (2013).
15. Jäncke, L. & Steinmetz, H. Brain size: a possible source of interindividual variability in corpus callosum morphology. in *Brain size: a possible source of interindividual variability in corpus callosum morphology* (ed. I.M. Zaidel E, Pascual-Leone A) 1–15 (Plenum Press, New York, 1998).
16. Josse, G., Seghier, M.L., Kherif, F. & Price, C.J. Explaining function with anatomy: language lateralization and corpus callosum size. *J Neurosci* **28**, 14132-14139 (2008).
17. Yarkoni, T., Poldrack, R.A., Nichols, T.E., Van Essen, D.C. & Wager, T.D. Large-scale automated synthesis of human functional neuroimaging data. *Nat Methods* **8**, 665-670 (2011).
18. Van Essen, D.C., *et al.* The WU-Minn Human Connectome Project: an overview. *Neuroimage* **80**, 62-79 (2013).
19. Shulman, G.L., *et al.* Right hemisphere dominance during spatial selective attention and target detection occurs outside the dorsal frontoparietal network. *Journal of Neuroscience* **30**, 3640-3651 (2010).
20. Shoval, O., *et al.* Evolutionary trade-offs, Pareto optimality, and the geometry of phenotype space. *Science* **336**, 1157-1160 (2012).
21. Thiebaut de Schotten, M., *et al.* Atlasing location, asymmetry and inter-subject variability of white matter tracts in the human brain with MR diffusion tractography. *Neuroimage* **54**, 49-59 (2011).
22. Karolis, V.R., *et al.* Reinforcement of the Brain's Rich-Club Architecture Following Early Neurodevelopmental Disruption Caused by Very Preterm Birth. *Cereb Cortex* **26**, 1322-1335 (2016).
23. Fieremans, E., Jensen, J.H. & Helpert, J.A. White matter characterization with diffusional kurtosis imaging. *Neuroimage* **58**, 177-188 (2011).
24. Jones, D.K., Knosche, T.R. & Turner, R. White matter integrity, fiber count, and other fallacies: the do's and don'ts of diffusion MRI. *Neuroimage* **73**, 239-254 (2013).
25. Myers, R.E. Organization of forebrain commissures. in *Functions of the Corpus Callosum* (ed. E.G. Ettlinger) 133–143 (CIBA Foundation Study Group 20, London, 1965).
26. Mazoyer, B., *et al.* Gaussian mixture modeling of hemispheric lateralization for language in a large sample of healthy individuals balanced for handedness. *PLoS One* **9**, e101165 (2014).
27. Thiebaut de Schotten, M., *et al.* A lateralized brain network for visuospatial attention. *Nat Neurosci* **14**, 1245-1246 (2011).
28. Zago, L., *et al.* The association between hemispheric specialization for language production and for spatial attention depends on left-hand preference strength. *Neuropsychologia* **93**, 394-406 (2016).
29. Schmahmann, J.D. An emerging concept. The cerebellar contribution to higher function. *Arch Neurol* **48**, 1178-1187 (1991).
30. Schmahmann, J.D. & Caplan, D. Cognition, emotion and the cerebellum. *Brain* **129**, 290-292 (2006).
31. Schmahmann, J.D. The Cerebrocerebellar System. in *Essentials of Cerebellum and Cerebellar Disorders: A Primer For Graduate Students* (ed. D.L. Gruol, Koibuchi, N., Manto, M., Molinari, M., Schmahmann, J.D., Shen, Y.) 101-115 (Springer International Publishing, Cham, 2016).

32. Liu, H., Stufflebeam, S.M., Sepulcre, J., Hedden, T. & Buckner, R.L. Evidence from intrinsic activity that asymmetry of the human brain is controlled by multiple factors. *Proc Natl Acad Sci U S A* **106**, 20499-20503 (2009).
33. Friedman, N.P. & Miyake, A. Unity and diversity of executive functions: Individual differences as a window on cognitive structure. *Cortex* (2016).
34. Cona, G.F., *et al.* Archetypes in human behavior and their brain correlates: An evolutionary trade-off approach. *bioRxiv* (2018).
35. Corbetta, M., Siegel, J.S. & Shulman, G.L. On the low dimensionality of behavioral deficits and alterations of brain network connectivity after focal injury. *Cortex* (2018).
36. Corbetta, M., *et al.* Common behavioral clusters and subcortical anatomy in stroke. *Neuron* **85**, 927-941 (2015).
37. Tzourio-Mazoyer, N., Joliot, M., Marie, D. & Mazoyer, B. Variation in homotopic areas' activity and inter-hemispheric intrinsic connectivity with type of language lateralization: an fMRI study of covert sentence generation in 297 healthy volunteers. *Brain Struct Funct* (2015).
38. Ghika-Schmid, F., van Melle, G., Guex, P. & Bogousslavsky, J. Subjective experience and behavior in acute stroke: the Lausanne Emotion in Acute Stroke Study. *Neurology* **52**, 22-28 (1999).
39. Azuar, C., *et al.* Testing the model of caudo-rostral organization of cognitive control in the human with frontal lesions. *Neuroimage* **84**, 1053-1060 (2014).
40. Siegel, J.S., *et al.* Re-emergence of modular brain networks in stroke recovery. *Cortex* **101**, 44-59 (2018).
41. Ramsey, L.E., *et al.* Normalization of network connectivity in hemispatial neglect recovery. *Ann Neurol* **80**, 127-141 (2016).
42. Joliot, M., *et al.* AICHA: An atlas of intrinsic connectivity of homotopic areas. *J Neurosci Methods* **254**, 46-59 (2015).
43. Tzourio-Mazoyer, N. & Seghier, M.L. The neural bases of hemispheric specialization. *Neuropsychologia* **93**, 319-324 (2016).
44. Luders, E., Thompson, P.M. & Toga, A.W. The development of the corpus callosum in the healthy human brain. *J Neurosci* **30**, 10985-10990 (2010).
45. Jennings, R.G. & Van Horn, J.D. Publication bias in neuroimaging research: implications for meta-analyses. *Neuroinformatics* **10**, 67-80 (2012).
46. Maier-Hein, K.H., *et al.* The challenge of mapping the human connectome based on diffusion tractography. *Nat Commun* **8**, 1349 (2017).
47. Girard, G., *et al.* AxTract: Toward microstructure informed tractography. *Hum Brain Mapp* **38**, 5485-5500 (2017).
48. De Benedictis, A., *et al.* New insights in the homotopic and heterotopic connectivity of the frontal portion of the human corpus callosum revealed by microdissection and diffusion tractography. *Hum Brain Mapp* **37**, 4718-4735 (2016).
49. Vu, A.T., *et al.* High resolution whole brain diffusion imaging at 7T for the Human Connectome Project. *Neuroimage* **122**, 318-331 (2015).
50. Avants, B.B., *et al.* A reproducible evaluation of ANTs similarity metric performance in brain image registration. *Neuroimage* **54**, 2033-2044 (2011).
51. Leemans, A. & Jones, D.K. The B-matrix must be rotated when correcting for subject motion in DTI data. *Magnetic Resonance in Medicine* **61**, 1336-1349 (2009).
52. Vos, S.B., *et al.* The importance of correcting for signal drift in diffusion MRI. *Magn Reson Med* **77**, 285-299 (2017).
53. Dell'acqua, F., *et al.* A modified damped Richardson-Lucy algorithm to reduce isotropic background effects in spherical deconvolution. *Neuroimage* **49**, 1446-1458 (2010).

54. Thiebaut de Schotten, M., *et al.* Damage to white matter pathways in subacute and chronic spatial neglect: a group study and 2 single-case studies with complete virtual "in vivo" tractography dissection. *Cereb Cortex* **24**, 691-706 (2014).
55. Dell'Acqua, F., Simmons, A., Williams, S.C. & Catani, M. Can spherical deconvolution provide more information than fiber orientations? Hindrance modulated orientational anisotropy, a true-tract specific index to characterize white matter diffusion. *Hum Brain Mapp* **34**, 2464-2483 (2013).
56. Wassermann, D., *et al.* The white matter query language: a novel approach for describing human white matter anatomy. *Brain Struct Funct* **221**, 4705-4721 (2016).
57. Kaiser, H.F. The varimax criterion for analytic rotation in factor analysis. *Psychometrika* **23**.
58. Chung, F. *Spectral Graph Theory* (American Mathematical Society, 1997).

## Supplementary materials

**Supplementary Table 1. Terms selected for the study**

acoustic	discriminative	insights	place	shifting
action	disgust	integrate	placebo	shifts
action observation	distance	integrated	placebo controlled	short term
actions	distraction	integrating	planning	signal task
addition	distractor	integration	pleasant	similarities
affective	distractors	integrative	pointing	similarity
ambiguous	distress	intelligence	position	size
anger	dorsal attention	intended	predict	skin
angry	duration	intention	predicted	sleep
anticipated	early visual	intentional	predicting	social
anticipation	eating	intentions	prediction	social cognition
anticipatory	economic	interference	prediction error	social cognitive
anxiety	effort	judgment	predictions	social interaction
appraisal	effortful	judgment task	predictive	social interactions
arithmetic	emotion	judgments	predicts	solving
arm	emotion regulation	language	preference	somatosensory
arousal	emotional	language comprehension	preferences	sound
articulatory	emotional faces	language network	preferential	sounds
association	emotional information	languages	preparation	space
associations	emotional neutral	learn	preparatory	span
associative	emotional responses	learned	primary auditory	spatial
attend	emotional stimuli	learning	primary motor	spatial attention
attended	emotional valence	learning task	primary sensorimotor	spatial information

attending	emotions	letter	primary sensory	spatial temporal
attention	empathic	letters	primary somatosensory	spatiotemporal
attention task	empathy	lexical	primary visual	speaking
attentional	empirical	lexical decision	prime	speech
attentional control	encode	limb	priming	speech perception
attribution	encoded	linguistic	probabilistic	speech production
audio	encoding	listened	probability	speech sounds
audiovisual	encoding retrieval	listening	probe	speed
auditory	endogenous	long term	prospective	spoken
auditory stimuli	episodic	maintain	pseudowords	spontaneous
auditory visual	episodic memory	maintained	punishment	stimulus driven
autobiographical	error	maintaining	reach	stop signal
autobiographical memory	errors	maintenance	reaching	storage
automated	estimation	match	reactivity	strategic
automatic	executive control	matching	read	strategies
autonomic	executive function	matching task	reading	strategy
aversive	executive functions	memories	reappraisal	stress
avoid	expectancy	memory	reasoning	stroop
avoidance	expectation	memory encoding	recall	stroop task
awareness	expectations	memory load	recognition	subtraction
belief	expected	memory performance	recognition memory	success
beliefs	explicit	memory processes	recognition task	successful
believed	exploration	memory retrieval	recognize	suffering
bias	expression	memory task	recognized	suppression
biased	expressions	memory tasks	recognizing	sustained

biases	external	memory wm	recollection	switch
binding	eye	mental imagery	rehearsal	switching
body	eye field	mentalizing	reinforcement	syntactic
calculation	eye fields	mnemonic	relational	tactile
capacity	eye movement	monetary	relevance	tapping
capture	eye movements	monetary reward	remember	target
categories	eyes	money	remembered	target detection
categorization	face	monitor	remembering	taste
category	face recognition	monitored	repeat	term memory
causal	face stimuli	monitoring	repeated	theory mind
choice	faces	mood	repetition	thinking
choices	facial	moral	repetition suppression	thought
choose	facial expression	motion	repetitive	thoughts
cognitive control	facial expressions	motivation	response inhibition	threat
cognitive emotional	familiar	motivational	response selection	threatening
coherence	familiarity	motor	responsiveness	time task
coherent	fear	motor control	retention	timing
color	fearful	motor imagery	retrieval	tom
combination	fearful faces	motor performance	retrieved	tone
combinations	feedback	motor response	reward	tones
combining	feeling	motor responses	reward anticipation	tool
communication	feelings	motor task	rewarding	tools
competing	finger	movement	rewards	touch
competition	finger movements	movements	rhythm	unfamiliar
comprehension	finger tapping	moving	risk	unpleasant
concept	flexibility	multisensory	risky	valence
concepts	flexible	music	rotation	valuable
conceptual	fluency	musical	rule	value
conditioned	food	names	rules	values



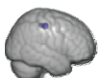
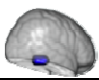
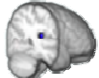

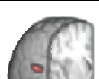


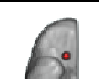




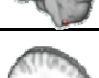
conditioning	foot	naming	saccade	verb
conflict	form	navigation	saccades	verbal
conflicting	forms	negative emotional	sad	verbal fluency
congruency	gain	neutral faces	saliency	verbal working
congruent	gains	neutral pictures	salient	verbs
congruent incongruent	gambling	neutral stimuli	search	video
conscious	game	nociceptive	secondary somatosensory	video clips
consciousness	gaze	nogo	seeking	videos
consolidation	gestures	noun	segregation	view
context	goal	nouns	selection	viewed
contexts	goal directed	novel	selective	viewing
contextual	goals	novelty	selective attention	violations
control processes	grasping	noxious	selectivity	virtual
coordination	hand	number	self	vision
covert	hand movements	numbers	self referential	visual
craving	hands	numerical	self reported	visual attention
cue	happy	object	semantic	visual auditory
cued	happy faces	object recognition	semantic information	visual field
cues	head	objects	semantic knowledge	visual information
decision	heard	observing	semantic memory	visual motion
decision making	hearing	oddball	semantics	visual perception
decision task	identification	oral	sensation	visual spatial
decisions	identity	order	sensations	visual stimuli
declarative	illusion	orientation	sensorimotor	visual stimulus
decoding	imagery	oriented	sensory	visual word
default mode	imagine	orienting	sensory information	visuo

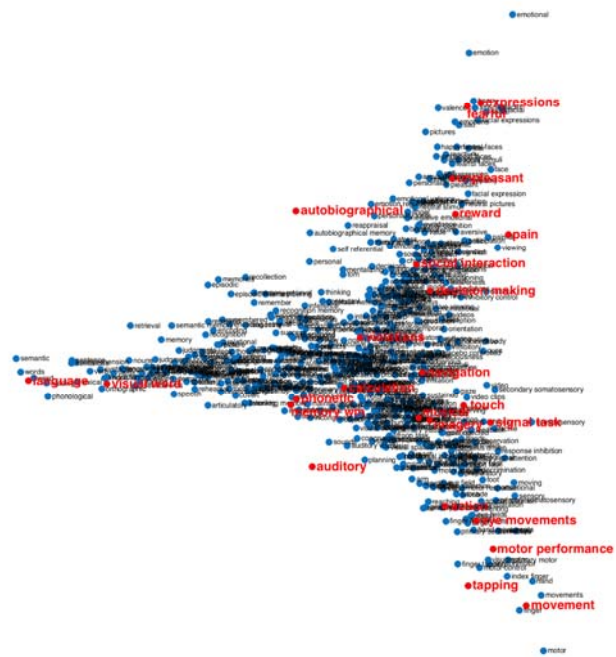


default network	imagined	orthographic	sensory modalities	visuomotor
delay	imitation	overt	sensory motor	visuospatial
delayed	implicit	pain	sentence	vocal
demand	impulsivity	painful	sentence comprehension	voice
demanding	incongruent	passive viewing	sentences	voluntary
demands	index finger	personal	sequence	wm
depth	induction	personality	sequences	wm task
detect	inference	personality traits	sequential	word
detected	inferences	perspective	serial	word form
detecting	inhibit	phonetic	series	word pairs
detection	inhibiting	phonological	sex	word recognition
detection task	inhibition	photographs	sexual	words
digit	inhibitory	picture	shape	work
discrimination	inhibitory control	pictures	shapes	working memory
discrimination task	insight	pitch	shift	written

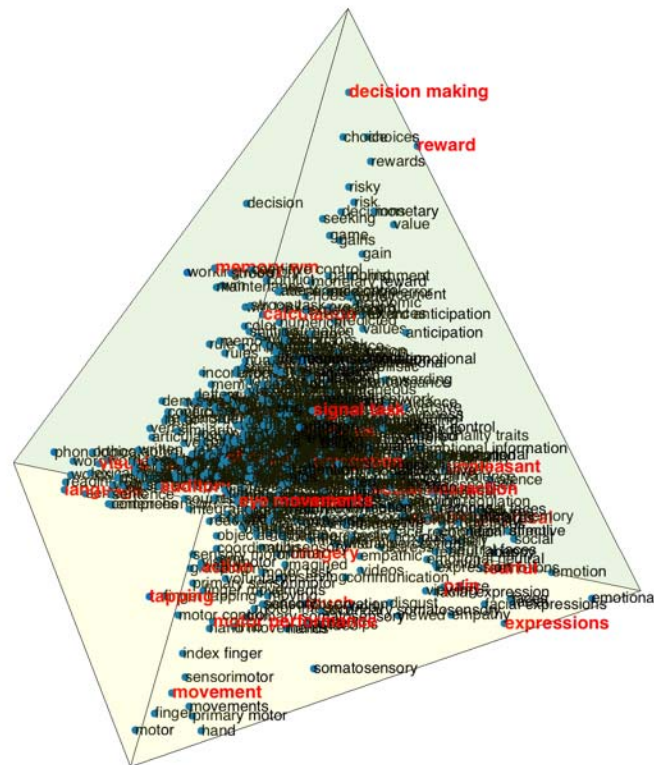
**Supplementary Table 2. Taxonomy of functional lateralisation**

Maps	PC labels	RH > LH				LH > RH			
		# voxels	T value	MNI X, Y, Z	Anatomical area	# voxels	T value	MNI X, Y, Z	Anatomical area
	Language	911	18.05	12,-78,-34	Crus II	2947	42.03	50,18,18	Prefrontal. C., extending into Precentral. G.
		45	12.45	28,28,50	Sup. Front S.	2607	40.59	58,-42,6	Mid. Temp. G. (posterior) & Supram. G. extending into Fusiform C.
		28	12.41	32,-96,6	Occipital pole	160	20.59	6,8,62	SMA (medial)
						102	18.03	40,-60,24	Sup. Temp. S., (posterior, deep)
						98	15.71	52,-8,-8	Sup. Temp. S. (middle- to-anterior segment)
	Movement	36	13.30	6,-56,-12	Area V	365	15.53	40,-14,60	Precentral G. (middle part)
		23	12.24	18,-50,-28	Area VI	149	16.35	10,-12,58	Border of Precentral G (medial) & SMA
						34	13.78	10,-44,76	Border of Sup. Par. L. & Postcentral G.
	Eye movement	120	16.50	20,-64,52	Sup. Par. L., bank of Intra-Par. S.	322	19.04	30,-48,56	Sup. Par. L.
		66	15.55	4,8,60	SMA (medial)				
		48	13.15	24,-8,52	Mid. Front. S. (posterior end)				
		25	13.77	24,-46,26	White matter				
		21	11.96	56,-40,38	Supram. G. (posterior)				
	Reward	23	11.41	14,10,-8	Putamen (inferior)	66	20.03	2,10,-2	Nucleus accumb.*
	Pain	107	17.53	52,-30,24	Planum temporale	36	13.36	62,-10,22	Postcentral G. (inferior)
	Auditory	60	11.90	58,-20,0	Sup. Temp. G. (posterior)	38	12.44	48,-34,20	Planum temporale
	Action (obser- vation)	74	14.48	62,-38,22	Supram. G. (posterior)	59	14.25	24,0,66	Sup. Front. G., (posterior)
						40	13.33	56,-22,38	Postcentral S. (inferior) & Supram. G. (anterior)
	Finger (tapping)	54	13.02	14,-62,-44	Area VIIIb	93	16.36	4,-6,60	SMA (medial)
						29	13.34	10,-20,8	Thalamus (posterior)
	Calculation /numerical	25	13.01	40,-50,42	IPS (lower bank)	59	14.75	36,-68,-38	Crus I
						35	14.14	20,-58,56	IPS (upper bank)
	Phonetic/ Speech perception	47	14.01	48,-24,2	Sup. Temp. S. (posterior, deep)	56	12.98	56,6,18	Precentral G.(inferior)
						20	11.68	62,-28,4	Sup. Temp. G. (posterior)

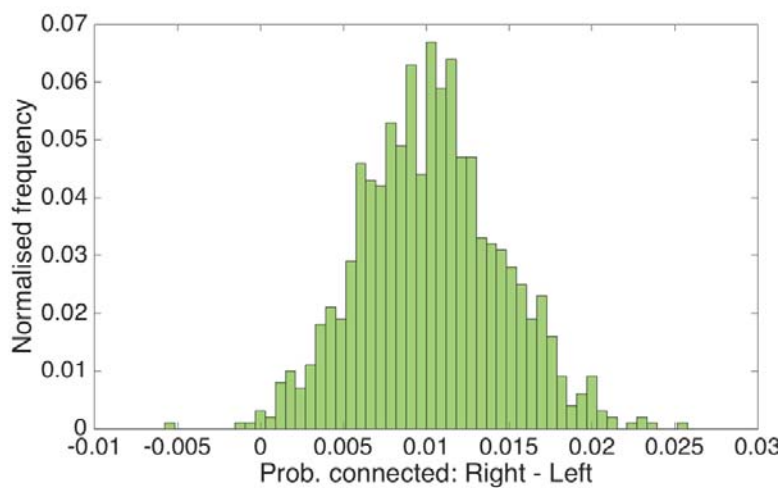
	<b>(Motor) imagery</b>	27	12.60	34,-10,72	Precentral G.	21	12.50	18,4,68	Sup. Front. G.
	<b>Autobiographical (memory)</b>					26	14.33	14,-52,16	Precuneus/anterior end of Par.-Occ. S.
	<b>Touch</b>					21	11.98	22,-16,-14	Hippocampus
	<b>Visual word/form</b>					92	14.32	34,-28,52	Postcentral G.
	<b>Music</b>					498	24.20	42,-42,-12	Fusiform cortex
	<b>Motor performance</b>					36	12.36	38,-26,18	Planum temporale
	<b>Facial expression</b>	100	14.87	52,-44,4	Sup. Temp. S.(posterior)				
		27	11.96	34,2,-26	Amygdala (inferior)				
	<b>Stop/ inhibition</b>	196	17.84	24,52,34	Anterior segment MFSulc / frontal pole				
		88	13.41	18,16,68	Sup. Front.G.				
		58	13.58	48,22,-2	Pars opercularis (inferior)				
	<b>Decision making</b>	44	14.19	14,28,-20	Medial Orbital G. (posterior)				
	<b>Working memory</b>	54	13.61	32,12,54	Mid. Front G. (posterior)				
	<b>Fearful (faces)</b>	82	17.09	30,0,-14	Amygdala (superior)				
	<b>(Un-) pleasant (faces)</b>	29	13.70	8,-50,-60	Area VIIIb				
	<b>Navigation</b>	50	12.70	36,-66,-50	Area VIIIb				
		38	11.99	28,-36,-14	Parahippocampal G. & Fusiform C.				
	<b>Social interaction</b>	48	12.89	44,10,-38	Temporal pole				
		24	11.90	44,-44,8	Sup. Temp S. (posterior end)				
	<b>Violations</b>	42	13.16	50,10,-30	Temporal pole				



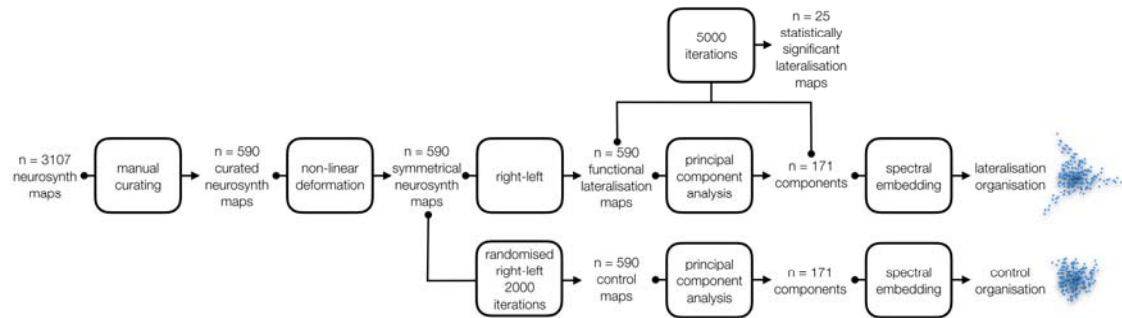
**Supplementary Figure 1.** Low dimensional structure of the functional lateralisation in the brain. Spatial embedding of all neurosynth terms in two dimensions revealing a triangular organisation with 3 apices: symbolic communication, perception/action, and emotion.



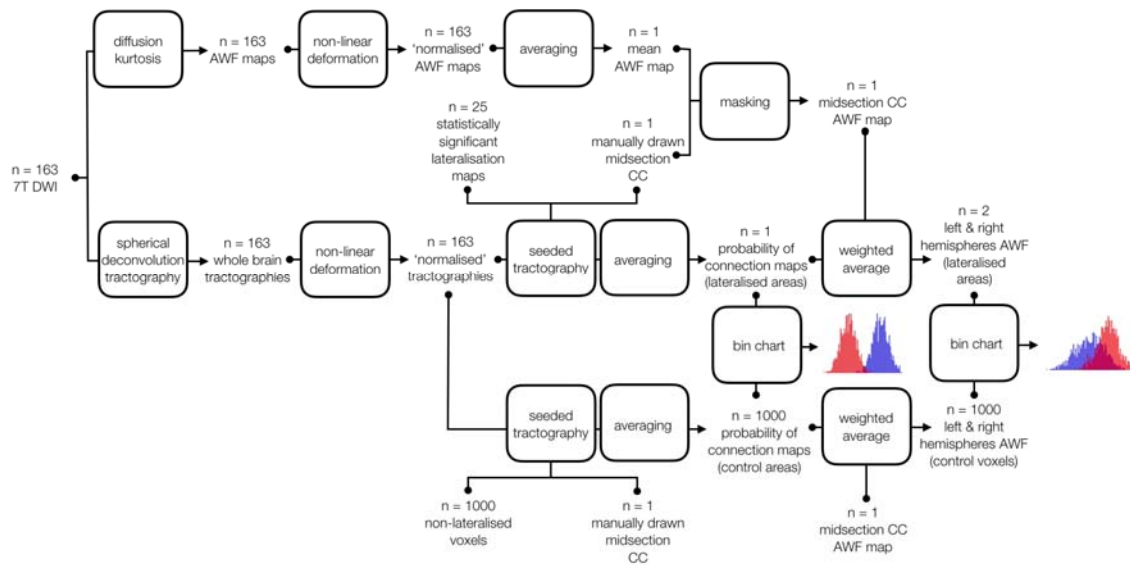
**Supplementary Figure 2.** Low dimensional structure of the functional lateralisation in the brain. Spatial embedding of all neurosynth terms in three dimensions revealing a tetrahedron organisation with 4 apices: symbolic communication, perception/action, emotion and decision making. (this is intended to be submitted as an interactive **3D.mat file**)



**Supplementary Figure 3.** Connectivity difference between right and left hemisphere in non-lateralised regions.



**Supplementary Figure 4.** Graphical summary of the global structure of functional lateralisation methods



**Supplementary Figure 5.** Graphical summary of the corpus callosum and functional lateralisation methods